



**HAL**  
open science

# Dislocation densities in a low-carbon steel during martensite transformation determined by in situ high energy X-Ray diffraction

Juan Macchi, Steve Gaudez, Guillaume Géandier, Julien Teixeira, Sabine Denis, Frédéric Bonnet, Sebastien Y.P. Allain

► **To cite this version:**

Juan Macchi, Steve Gaudez, Guillaume Géandier, Julien Teixeira, Sabine Denis, et al.. Dislocation densities in a low-carbon steel during martensite transformation determined by in situ high energy X-Ray diffraction. *Materials Science and Engineering: A*, 2020, 800, pp.140249. 10.1016/j.msea.2020.140249 . hal-02943929

**HAL Id: hal-02943929**

**<https://hal.science/hal-02943929>**

Submitted on 30 Sep 2020

**HAL** is a multi-disciplinary open access archive for the deposit and dissemination of scientific research documents, whether they are published or not. The documents may come from teaching and research institutions in France or abroad, or from public or private research centers.

L'archive ouverte pluridisciplinaire **HAL**, est destinée au dépôt et à la diffusion de documents scientifiques de niveau recherche, publiés ou non, émanant des établissements d'enseignement et de recherche français ou étrangers, des laboratoires publics ou privés.

# **Dislocation densities in a low-carbon steel during martensite transformation determined by In situ High Energy X-Ray Diffraction**

## **Authors**

Macchi Juan<sup>1</sup>, Gaudez Steve<sup>1</sup>, Geandier Guillaume<sup>1</sup>, Teixeira Julien<sup>1</sup>, Denis Sabine<sup>1</sup>, Bonnet Frédéric<sup>2</sup>, Allain Sébastien Y.P<sup>1</sup>

<sup>1</sup> Institut Jean Lamour, UMR 7198 CNRS Université de Lorraine, Campus ARTEM Nancy, France

<sup>2</sup> ArcelorMittal Research SA, APRC, Voie Romaine, BP 30320, 57283 Maizières les Metz, France

**Keywords:** Steel ; Martensite ; Synchrotron ; X-ray analysis; Dislocation ; Mechanical behavior

## **Corresponding author:**

Macchi, Juan

[juan.macchi@univ-lorraine.fr](mailto:juan.macchi@univ-lorraine.fr)

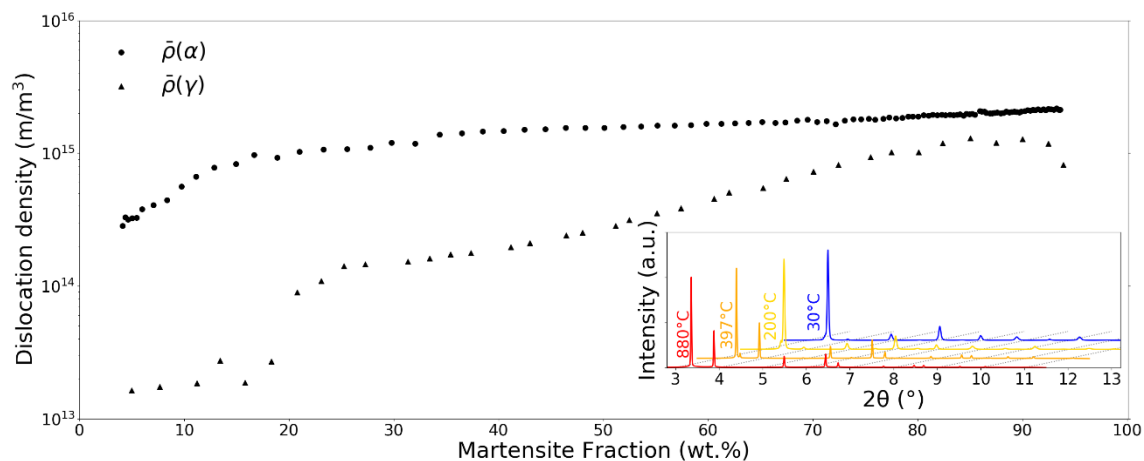
Tel.: +33 03 72 74 26 87

Postal address: Campus Artem, 2 allée André Guinier, 54011 Nancy

## Abstract

The evolution of the dislocation densities in martensite and in austenite during the quench of a low-carbon (0.215 wt.% C) steel is investigated in situ by the mean of a High Energy X-Ray Diffraction experiment on a synchrotron beamline. The line configuration offers an excellent time resolution well adapted to the studied martensitic transformation kinetics. The mean density of dislocations in martensite increases as the transformation proceeds confirming that dislocations are not homogeneously distributed between the laths in agreement with some recent post-mortem observations. The resulting spatial distribution of dislocations and the associated strain-hardening support the views assuming that lath martensite is a heterogeneous microstructure and behaves as a “multiphase” aggregate. In austenite, the increase in dislocation densities is even more significant meaning that austenite in martensite is also a hard phase, contradicting some recent theories attributing to films of retained austenite a major role in the plasticity of martensite.

## Graphical Abstract



## Highlights

- In situ High Energy X-Ray Diffraction experiments have been conducted during a quenching experiment to determine at the same time the progress of the martensitic transformation and the densities of dislocations in both phases (martensite and austenite).
- Post-processing the history of the measurements in both phase during the transformation allows to isolate the dislocation density in the newly formed martensitic laths. This provides the complete distribution of dislocation densities in the final microstructure.
- The distribution of local yield strength resulting from the dislocations is found to be a first order contribution to explain the mechanical behavior of martensite.
- Very high dislocation densities are also found in the residual austenite pointing out that this latter should be probably as hard as martensite laths.

## Introduction

Although lath martensites are one of the key microstructure constituents of conventional steels, of hot-stamped boron-bearing steels and also of several 3<sup>rd</sup> generation multi-phased steels for automotive construction [1], the correlation between their mechanical behavior and their specific hierarchical microstructure is not completely established yet. A major reason is that most of the studies have considered martensite as an homogeneous structure. Recent works in this field have tried to highlight that martensite microstructures are in fact dispersed in terms of size, residual stresses, defects and composition and behave like a multiphase aggregate [2–4]. These results sustain thus the micromechanical approach considering martensite as a continuum composite material (CCA) [2,3] proposed by the present authors already in 2012 and assuming a distribution of local yield strengths at the microstructure scale. Since then, this interpretation has been supported either by local mechanical measurements or by direct microstructure observations.

Some authors have found a wide dispersion of the mechanical properties between different martensite laths thanks to nanohardness investigations. Li et al. [5] showed that the

nanohardness within the martensite studied can vary between 5 GPa and 11 GPa. It has been observed that the smaller blocks (aggregate of laths with low angle misorientation) have a higher hardness in [6] with an average nanohardness of about 5.5 GPa for the large blocks and 6.9 GPa in the small blocks with a width estimated by Electron Backscattered Diffraction (EBSD) equal to 6 and 3.5  $\mu\text{m}$  respectively. He et al. [7] studied ferritic microstructures (ferrite, lower and upper bainite, and martensite) highlighting a significantly wider scattering in the martensite results. In addition a high heterogeneity in the deformation of this phase was reported in [8] by digital image correlation based on successive EBSD cartographies taken during the test. The heterogeneity was reported to increase with deformation indicating strain localization and indicating a huge dispersion in the local yield strengths of the laths.

These local dispersions and the resulting composite behavior are related to the martensite transformation itself, which is essentially displacive and athermal. Very few studies have been dedicated to the formation of microstructure heterogeneities in martensite. Starting from post mortem observations, Morsdorf et al. [9] have analyzed how the martensite microstructure appears progressively. The study shows the presence of a wide dispersion of thickness, with thin laths (from  $\approx 50$  to  $\approx 500$  nm) and coarse lath, up to  $\approx 3.5\mu\text{m}$ . A quantitative analysis by atom probe tomography in thin and coarse laths reveals that carbon segregation is more intense in the coarse laths than in the thin ones. Nanohardness characterization presented in the same work shows that the thinner laths were  $\approx 10\%$  harder than the coarse ones. It suggests that the first martensite blocks/lath to appear will be the largest, the most segregated and the softest. On the contrary, the last structures to form will be the hardest domains of the microstructure [9]. Similar conclusions were drawn by Badinier et al. [10,11].

To the authors' best knowledge, Christien et al. [12] were the only group to study in situ the evolution of the mean dislocation density during the martensite transformation in both martensite and austenite. The study was conducted by neutron diffraction and the studied steel was a carbon-free stainless steel permitting long acquisition time (1 pattern every 2 mins). Results showed that the higher the martensite phase fraction, the higher the mean dislocation densities in both phases.

The present work consists also in the detailed characterization of the evolution of mean dislocation density in both martensite and austenite phases in situ during the transformation. We have addressed the challenge to follow these evolutions in a low carbon steel in which martensitic transformation is faster and can be accompanied by self-tempering mechanisms. A set-up with an excellent time resolution suitable for these particular steels and transformation

kinetics (1 pattern every 0.1s) was used. Moreover, an analysis to determine in the final microstructure the associated spatial dispersion of local hardening due to these dislocations was developed. This new insight permits to go farther in the understanding of the mechanical properties of this heterogeneous phase.

## **Material and methods**

An industrial low-carbon alloyed steel, provided by ArcelorMittal Maizières Research Center, France, with a composition Fe-0.215C-0.25Si-1.82Mn-0.18Cr wt.% was investigated. The steel was received after the cold-rolling stage (1.5 mm thickness) and samples were machined by 10 mm x 4 mm x 1.5 mm plates. No surface preparation was performed.

High Energy X-ray diffraction (HEXRD) experiments were performed in situ at the Deutsche-Elektronen-Synchrotron (DESY, PETRA-III) P07 beam line with a monochromatic beam with an energy of 100 keV ( $\lambda=0.012398$  nm) allowing to work in transmission mode. The association with a fast 2D Perkin-Elmer detector enabled high acquisition rates (10 Hz) needed to study fast processes on bulk samples (400 x 400  $\mu\text{m}$  beam size by 1.5 mm thickness) with a sufficient time resolution, as it is the case of the martensitic transformation in low carbon steels. The detector was positioned about 1.5 m behind the sample, giving access to full Debye-Scherrer rings with a maximum  $2\theta$  angle of  $8^\circ$  (5 Debye Scherrer rings per phase).

Martensitic quench treatment was performed with a modified Bähr DIL805 A/D dilatometer available on the beam line. The heat treatment used to investigate the martensite transformation consists of a heating at  $20^\circ\text{C/s}$  up to  $880^\circ\text{C}$ , followed by an isothermal holding during 180 s and finally of a fast cooling by argon gas blowing (aiming at a cooling rate of  $50^\circ\text{C/s}$ ) down to the room temperature. The austenitization heat treatment leads to a mean prior austenite grain size of  $6.5\ \mu\text{m}$ . This value has been determined by Prior Austenite Grain reconstruction using Decrypt® software on the basis of EBSD cartographies (results not shown here). For the studied cooling, 500 diffraction patterns have been acquired between the  $M_s$  temperature ( $394^\circ\text{C}$ ) of the alloy and the room temperature.

The 2D diffraction patterns produced during the experiments were integrated circularly using pyFAI python library [13]. The deduced 1D diffractograms (Intensity vs  $2\theta$ ) were analyzed with a Rietveld refinement procedure using pseudo-Voigt functions to reproduce diffraction

peaks. The Rietveld method here has served to obtain the phase fractions with an uncertainty of  $\pm 1\%$  (absolute value) during the martensitic transformation. According to 1D diagrams, two phases were considered during the analysis: martensite with a body centered tetragonal structure ( $I4/mmm$ ) and austenite with a cubic face centered structure ( $Fm-3m$ ). No carbide (transition iron carbides and/or cementite) resulting from martensite self-tempering was detected during the quench by HEXRD, even if such configurations is known to enable their detection if present in low amount [14]. Three experiments have been conducted in order to ensure the repeatability.

For simplicity, and to avoid redundancy, only one experiment is presented and discussed in the present paper. The other experiments show strong similarity with the one presented here, and the same conclusions would be extracted from each investigation. Nevertheless, the results of each individual experiments are available in the supplementary data.

Since the pioneer works of Williamson & Hall [15], it is well known that dislocations present in polycrystals will affect the width of their diffraction peaks. The higher the dislocation density (resp. the lower the crystallite size), the larger the peak width [16]. The Rietveld method does not permit to determine properly the Full Width Half Maximum ( $FWHM(2\theta)$ ) of each diffraction peaks as it is only a mean description of a full line profile. In fact, the FWHM in Fullprof is based on the Caglioti et al.'s theory [17] which required the refinement of three parameters per phase to describe the mean FWHM for each of its peak. This description does not permit to account in particular for the respective crystallographic anisotropy of the phases as suggested by Ungar et al. [18].

Besides the Rietveld refinement of the full diffractograms, a separate refinement has thus been conducted peak by peak using Pearson VII functions in order to obtain the individual FWHM and angular position of the phase diffraction peaks. The instrumental contribution to the peaks broadening was measured with a silicon powder and subtracted from the measured FWHM by considering a square additive law [19]. The instrumental contribution was considered constant during the proposed experiments accounting for the stability of the beam during each experiment and considering that the only parameter that changes is the temperature of the sample, no movement has been made even on the sample or the detector.

While a tetragonal cell was used for the Rietveld refinement, it was not possible to model each peak individually considering tetragonality with one Pearson VII function per diffraction plane family. The diffraction peaks were then fitted with a single symmetric Pearson VII

function. This introduces an over estimation in the dislocation density as the peaks will be slightly larger than expected due to the tetragonal lattice. At the end of the martensitic transformation, one diffractogram was analyzed both by a single function per diffraction peak and by one Pearson VII function per diffraction plane families considering tetragonality imposing the difference between positions due to the  $c/a$  determined by the Rietveld refinement (1.006). For clarity, in the case of the peak (200) the diffraction plane families are (hk0) and (00l) and the effect of the tetragonality (1.006) in the experimental set-up produces a difference of  $0.03^\circ 2\theta$  between both families. The dislocation density found in the second case was only 12% lower than only considering one function by peak. The error introduced considering a single peak instead of two for the fitting procedure is low in regard to the experimental uncertainties for the low carbon steel studied and would not modify the tendencies found and conclusions extracted.

From the instrumentally-corrected FWHMs, the dislocation densities in martensite and in austenite for each studied diffraction patterns were estimated by the modified Williamson-Hall method (mWH), introduced by Ungár et al. [18]. This method imposes a contrast factor for each refracting plane family considering the anisotropy of the material [20]. Under the assumption that the only feature introducing broadening in the materials reflections are the dislocations and crystallite sizes, the peak broadening can be described by the following equation:

$$\Delta K = \zeta/D + (((\pi M b^2)/2)^{1/2} * \bar{\rho}^{-1/2}) * K * \bar{C}_{hkl}^{1/2} + O K^2 \bar{C}_{hkl} \quad (1)$$

where  $\Delta K = \text{FWHM}(\theta) * 2 \cos(\theta) / \lambda$ ,  $K$  is the norm of the scattering vector defined by  $K = 2 \sin(\theta) / \lambda$ ,  $D$  is the crystallite size,  $M$  is a parameter depending on the dislocation density,  $b$  is the Burgers vector,  $\bar{\rho}$  is the mean dislocation density and  $\bar{C}_{hkl}$  is the average contrast factor of dislocations for the specific reflection.  $O K^2 \bar{C}_{hkl}$  is a higher order term with no meaning established [21], where  $O$  is much smaller than the coefficient before  $K \bar{C}_{hkl}$ , and it is not considered here [22]. For the present work  $\zeta$  was set equal to 0.9 as done in [15] and  $b$  to  $2.5 \cdot 10^{-10} \text{m}$  (ca.  $2.49 \cdot 10^{-10} \text{m}$  and  $2.517 \cdot 10^{-10} \text{m}$  respectively for the ferrite and the austenite) for both phases analyzed.  $M$  is a dimensionless parameter linked to the outer cut-off radius of the dislocations and the dislocation arrangement inside the phase, this parameter can be evaluated with the Warren-Averbach method. In the present study this parameter was considered constant during the thermal treatment. While it can vary [19], it is set at 2.2 considering the average value from [23].

The dislocation contrast factor for each reflection ( $\bar{C}_{hkl}$ ) is taken from ANIZC software [24] which gives the theoretical contrast factor for screw and for edge type dislocations. It accounts from the type of lattice (considered as cubic here), the second order elastic constants and reflections [24]. The slip systems considered for edge dislocation are  $\langle 111 \rangle \{110\}$  and  $\langle 110 \rangle \{111\}$  respectively for the body-centered and face-centered-cubic phases. The dislocation lines considered for screw are  $\langle 111 \rangle$  and  $\langle 110 \rangle$  respectively for the body-centered and face-centered-cubic. As the elastic constants ( $C_{11}$ ,  $C_{12}$  and  $C_{44}$ ) vary with the temperature [25–27], the dislocation contrast factors vary as well. The dislocation contrast factors for screw and edge type dislocations are considered as temperature dependent and have been calculated using the values in the literature for ferrite [25–27]. For austenite, they have been considered constant due to the lack of available data [28]. Many models propose a description of isotropic elastic constants but the data considering the elastic anisotropy of the lattice are rare. However, as the phases are considered separately in this second post-treatment, the error made in austenite has not effect on the results for martensite

Table 1 shows the dislocation contrast factor calculated at room temperature for both martensite and austenite considering a ratio of 50% edge and 50% screw type dislocations as [19]. The contrast factor evolutions with temperature for martensite were calculated up to 700°C and fitted with a second order polynomial function ( $aT^2 + bT + c$  with T in K). For the  $\{200\}$  reflection fitted parameters are  $a=1.73 \cdot 10^{-7}$ ,  $b=4.854 \cdot 10^{-5}$  and  $c=0.277$  while for  $\{211\}$   $\{220\}$   $\{321\}$  they are  $a=2.266 \cdot 10^{-8}$ ,  $b=7.042 \cdot 10^{-7}$  and  $c=0.1408$  for the considered proportion of dislocation types.

An estimation of the error introduces by neglecting the elastic constants thermal dependence was performed on the martensite phase at 350 °C. The dislocation density was found 7% lower than accounting for the thermal dependence. The influence of this sensitivity in thus limited in the studied temperature range. Based on this result, we could expect similar results for austenite in the investigated temperature range (between Ms down to RT).

Table 1: Dislocation contrast factors at room temperature for both ferrite and austenite considering a ratio of 50% edge and 50% screw type dislocations.

Ferrite	$\{200\}$	$\{211\}$	$\{220\}$	$\{321\}$
$\bar{C}_{hkl}$	0.278	0.141	0.141	0.141
Austenite	$\{200\}$	$\{220\}$	$\{311\}$	$\{420\}$
$\bar{C}_{hkl}$	0.299	0.148	0.204	0.202

In order to estimate an error introduced by the possible texture of the steel and the experimental scattering, one 2D image (Debye Scherrer rings) from the end of the quench was integrated circularly each degree yielding to 360 1D diagrams. Each diagram was analyzed with the mWH procedure. The calculations (results not shown here) show that 95% of the dislocations densities calculated, for both martensite and austenite phases, were in between the mean value and  $\pm 22.5\%$  (i.e. the dispersion from the mean value for two standard deviations (95%) was lower than  $\pm 22.5\%$ ).

## Results:

The cooling curve of the most representative in situ experiment is presented in Figure 1(a) with the corresponding dilatometric signal. The first evidence of martensitic transformation is observed on the dilatometric curve due to the transformation strain from austenite to martensite. In addition, as martensitic transformation is by nature an exothermic reaction, it affects the thermal evolution. The apparent martensite start temperature ( $M_s$ ) was found equal to  $394 \pm 4^\circ\text{C}$  by the analysis of 3 dilatometric curves and applying the offset method proposed by Yang and Bhadeshia [29]. This temperature corresponds also to a deviation in the temperature evolution (sudden change in slope). Nevertheless, in the studied condition, the transformation appears to be sluggish at the beginning as only 5% of martensite is formed at  $360^\circ\text{C}$ . These points will be clarified and discussed later at the light of the XRD data.

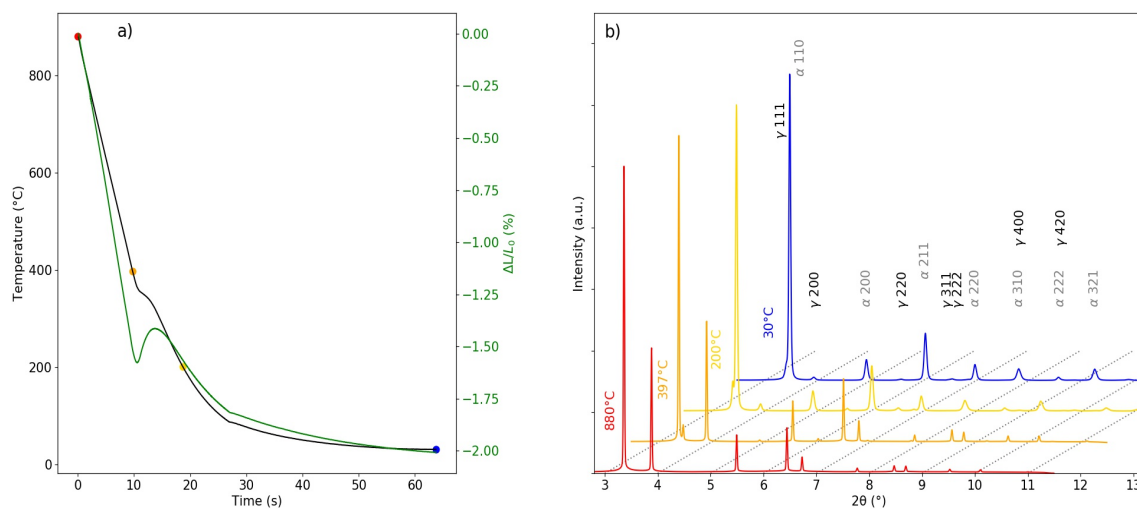


Figure 1: a) Cooling and dilatometric curves as function of time and b) 1D diffractograms recorded during the HEXRD in situ experiment corresponding to the temperatures highlighted on the cooling curve, respectively 880, 394 ( $M_s$ ), 200 and 30 °C. The deformation and the time were set at 0 at the end of the austenitization stage.

Some selected 1D diffractograms of the same experiment are presented in Figure 1(b) They correspond to the conditions highlighted by dots in Figure 1(a). The same color code has been followed. The respective reflections of austenite and martensite are indicated ( $\alpha$  standing for ferrite and martensite and  $\gamma$  for austenite). Along the cooling sequence, the alloy is first fully austenitic at 880°C. At the apparent Ms temperature (394°C), the diffraction pattern shows already the presence of small fraction of ferritic phase (<5wt.%). This fraction is attributed to a ferritic or a bainitic transformation prior to the martensitic transformation. At 200°C and at RT, the alloy is mainly martensitic. The martensite phase fraction measured at room temperature is 94 wt.% and is similar between the experiments, meaning that 6 wt.% of austenite is retained at RT.

Figure 2 presents the progress of the martensitic transformation, i.e. the martensite weight fraction evolution during the quench as a function of the temperature by XRD. The transformation kinetics obtained by dilatometry have been plotted from 0 (before the start of the transformation) to 100 (end of detected transformation) in the same figure. The values measured by XRD encompass all ferritic phases (possible ferrite transformation before Ms and martensitic transformation). Both methods show that the transformation kinetics is initially not following a kinetics as it could be predicted by Koistinen and Marburger and then a rapid transformation is observed. The sudden increase in the transformation kinetics by the Rietveld analysis occurs around 365°C which is 32°C lower than the apparent Ms reported above. This second value agrees well with the theoretical Ms temperature of the investigated steel (369°C) accounting for the nominal steel composition and the prior austenite grain size (PAGS) [30,31]. This two steps transformation is common in industrial steels and is often explained by microsegregations or decarburized surface layer which affect the local transformation start temperature [32,33]. As a consequence, there is a spatial and time distribution of the transformation progression. The transformation starts earlier in microstructure regions where the Ms is high (low C, low Mn, high PAGS) and later where Ms is lower. In the following, 365°C will be considered as the true Ms temperature of the alloy considering it represents better the value of the alloy mean composition.

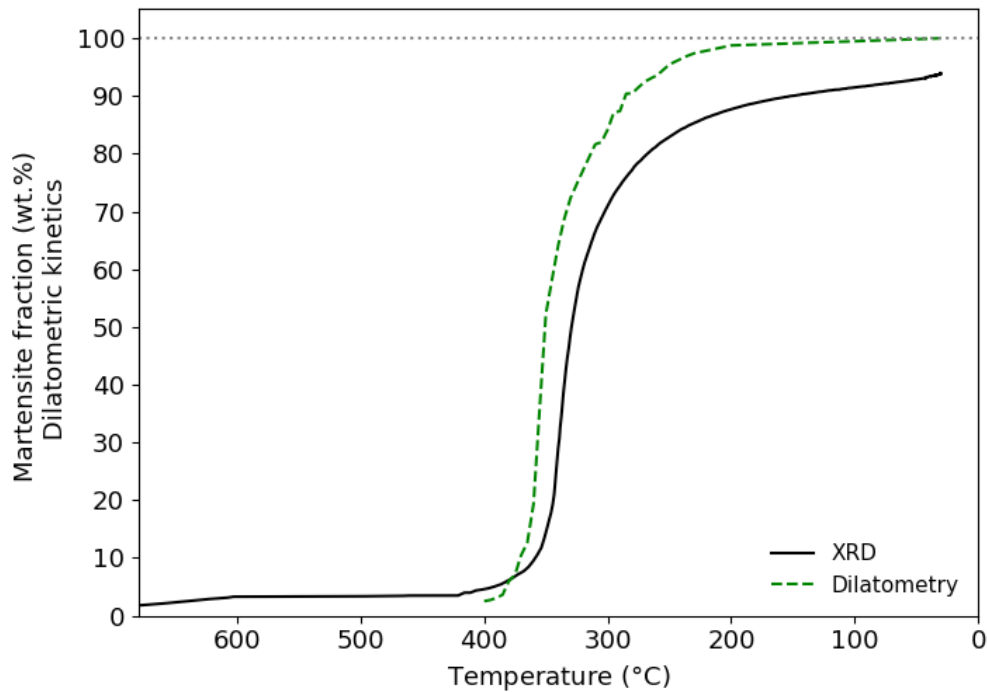


Figure 2: body-centred phase fraction determined by XRD and martensite fraction measured by dilatometry as function of the temperature during the quench. The fractions obtained by dilatometry were calculated from the transformation kinetics and considering the start and end fractions equal to the XRD measurements.

Figure 3(a) shows the relative change in the FWHM of austenite/retained austenite and martensite peaks during the quenching treatment as a function of the temperature. The values have been normalized by the position of the studied peaks. During the cooling between the austenitization temperature down to the  $M_s$  temperature, the FWHM of austenite is almost constant as expected, meaning no change in crystallite size and defect density in the absence of phase transformation and plastic events. The observations are consistent with the literature [12,34]. The cooling rate is too high to enable recovery process. During the first stage of martensite transformation (not following the Koistinen and Marburger's athermal equation), between 394 and 365°C, no notable changes are observed while below 365°C the austenitic FWHMs of all diffraction peaks increase drastically. As the martensite transformation progresses, the austenite FWHMs continue to increase down to the room temperature. For martensite, the observed behavior is rather different. Due to very low peak intensities at the beginning of the transformation, up to 5 wt.% of body-centered phase, the uncertainties are high. The measured FWHMs are thus not relevant down to 365°C. Below this true  $M_s$

temperature, a strong increase in the FWHMs is observed. Then the increase slows down when ca. 40 wt.% of martensite is formed, at ca. 350°C.

Different evolutions of the peak broadening with the temperature are experimentally observed for the austenite and for the martensite. A more gradual increase is presented in the former whereas martensite seems to saturate at an early stage of the transformation. While the authors cannot give at the moment a full explanation of the presented different behaviors some elements can be numbered:

- The saturation of the FWHM of the martensite could be partially related to the increase of the martensite fraction, i.e. a newly fraction of martensite with a high FWHM will produce a bigger increase on the average FWHM when the total martensite fraction is low than when martensite fraction is high. A similar reasoning can be postulated for the austenite; as the percentage of the phase decreases the increase of the FWHM in a fraction of the residual phase produces a more important effect on the average FWHM.
- The continuous increase of the FWHM of the austenite might be also a consequence of the martensitic transformation of the austenite with lower dislocation density. Although the high deformed austenite is less stable from a thermodynamic consideration, the crystal defects can mechanically stabilize the mother phase [35]. The transformation of the austenite with a lower dislocation density produces an increase of the average dislocation density observed.
- The increase of the peak broadening of the austenite at the final states of the transformation might be also related to the presence of distributions of internal stresses as reported in [36]. The progressive confinement of austenitic regions makes relaxation mechanisms more and more difficult, increasing the residual stresses.

Let us mention that during phase transformation the interpretation of the FWHM is complex since it is affected by several contributions: crystal defects, crystallites size (size of diffraction domains), thermal, chemical and internal stresses heterogeneities within the phases/grains, free surface effects. Due to the set-up used to investigate martensite transformation (transmission mode through the 1,5 mm thickness of the sample), the sample surface effect is low and assumed negligible. In addition investigations showed that the mean crystallites size of both phases are mostly constant. Presently, as the transformation is displacive, no chemical composition distribution is considered (we do not take into account possible self tempering during the martensite transformation). However, there are internal stresses in the phases

resulting from the martensitic transformation during cooling due to the phase transformation deformations and their precise knowledge at the different scales is complex and is still an open question. At the scale of the phases, the mean internal stresses generated during martensitic transformation have been clearly evidenced experimentally by HEXDR [34,37,38]. They are hydrostatic and lead to a shift of the diffraction peaks of the phases.

Internal stress heterogeneities in the martensitic microstructure have been fewly addressed in literature. Thus, on one hand, Archie et al. [39] and Fukui et al. [40] recently reported an anisotropic strain distribution by SEM-FIB based ring-core method at the scale of the martensite variants, while Nakada et al. have reported an anisotropic distribution of the micro residual strains in the austenite [36]. It is possible to assume that the effect of the internal stresses on the FWHM might become more important with the progress of the transformation as the size effect is more important.

In our case, the experimental method used is not able to deconvolute internal stress heterogeneities from the dislocation density contribution within the phases. Nevertheless, the high contribution of the dislocation density to the FWHM in the martensite is supported by the good correlation of the values of dislocation densities measured by TEM and HEXRD in the literature [41] and by our own investigations (TEM:  $8 \times 10^{14}$  1/m<sup>2</sup>, HEXRD:  $2 \times 10^{15}$  1/m<sup>2</sup>). In our approach we will link the evolutions of FWHM to the evolutions of dislocation densities in both phases.

The Figure 3(b) shows the mean dislocation densities ( $\bar{\rho}$ ), deduced from the FWHMs shown in Figure 3(a) with the modified Williamson-Hall method, in martensite ( $\alpha$ ) and austenite ( $\gamma$ ) as a function of the martensite fraction during the quench. The data have been plotted as a function of the martensite fraction instead of the temperature. As the martensite transformation proceeds, the dislocation density increases both in martensite and in austenite as reported in [12]. This is obviously related to the displacive nature of the martensitic transformation and the accommodation of the phase transformation strain which affects both the transformation product and the austenitic matrix in which the transformation occurs. (Please note that the densities have been plotted in a log scale).

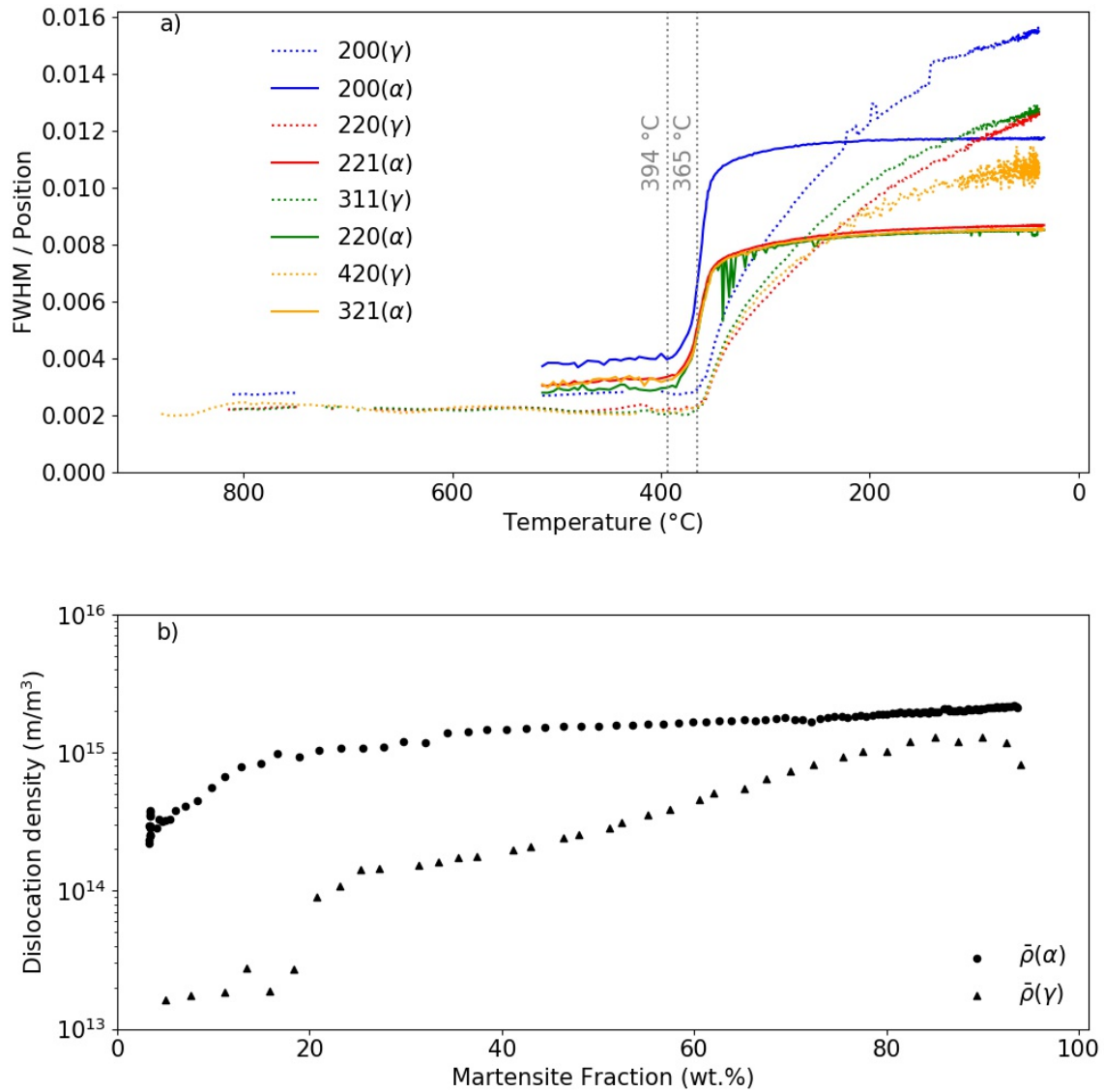


Figure 3: a) FWHMs of austenite (dotted lines) and martensite (continuous lines) diffraction peaks as function of the temperature during the whole studied cooling sequence (after austenitization down to room temperature) and b) deduced mean dislocation densities in both martensite (circle) and austenite (triangles) as a function of the transformed martensite phase fraction.

At the beginning of the martensite transformation, preexisting bcc phase shows already a high density of dislocations ( $2 \cdot 10^{14} \text{ m/m}^3$ ). This value lets us suspect that the observed ferritic phase observed prior the martensitic transformation (above  $394^\circ\text{C}$ ) corresponds in fact to bainitic ferrite appearing just before the martensitic transformation. During the first 20% of the martensitic transformation (mainly occurring below  $365^\circ\text{C}$ ), the dislocation density increases drastically to reach a value close to  $9 \cdot 10^{14} \text{ m/m}^3$ . During the rest of the

transformation, down to room temperature, the density of dislocations continues to increase but at an apparent lower rate, to reach a final value of  $2 \cdot 10^{15} \text{ m/m}^3$ . This value is in good agreement with the values generally reported at RT in low carbon martensitic steels [42,43]. By TEM observations in a Fe-0.18C steel, Morito et al. reported for instance mean densities around  $1.1 \cdot 10^{15} \text{ m/m}^3$  [41]. The mean dislocation density in martensite phase is thus 10 times higher at the end of the transformation compared to the very first 5 wt.% transformed. It should be emphasized that the dispersion of values along the transformation is lower than in the study of Christien et al. [12]. This has been permitted by our faster acquisition rate (10 Hz). At the fastest transformation rates (around 350°C), diffractograms and thus dislocation densities are measured every 2.5% of transformed martensite. The evolution of the dislocation density of the martensite does not present a linear tendency as reported by Christien et al. [12], thus, a square root function was chosen to fit the experimental data by its simplicity and general acceptable fit as can be observed in Figure 4.

The evolution of the dislocation density in the austenite does not saturate before 80 wt.% of martensite is formed. The evolutions in austenite and in martensite seem correlated. Before the martensitic transformation, the density is  $1.7 \cdot 10^{13} \text{ m/m}^3$  as expected from an austenitic phase annealed at high temperature. The density increases during the first 15% of transformation to reach  $8 \cdot 10^{13} \text{ m/m}^3$ . After this apparent first fast regime, the density continues to increase very rapidly but at almost the same rate. It should be noted that the data scattering is higher in austenite than in martensite at the beginning of the transformation. This is related to the low density values reported in that case. However, the measured values do not evolve much during the cooling before the martensitic transformation, as shown in Figure 3(a). This permits to ascertain the determination procedure described above, as no plastic events are expected in austenite.

## **Discussion**

The discussion will be segmented in three parts. The first will focus on the insight brought by the dislocation density measurements in the martensite phase during cooling. The succeeding section will analyze the effect of the dislocation density on the austenite strength and the last one is dedicated to analyze the distribution of local and spatial yield strength distribution in martensite due to the distribution of dislocation densities.

### Instantaneous dislocation density in martensite:

The studied steel shows at room temperature a very conventional lath martensitic microstructure as observed by [9] on similar steels. It is now well admitted that this typical microstructure appears in a displacive way by the nucleation of new laths; gathered into blocks of similar variants and packets of coplanar variants inside prior austenite grains [9]. As said in the introduction, the size, the dislocation structure, the segregations, the residual stresses and thus the local strength of these laths at room temperature should strongly depend on their respective transformation temperatures.

As a consequence, it is likely that the dislocations are not homogeneously distributed in the final martensitic microstructure.

The increase in the mean dislocation density in martensite during the transformation can be interpreted either by the fact that already formed laths undergo plastic deformation or by the fact that new laths present a higher dislocations density than the previous ones arising the mean value. The plastic deformation in already formed lath structures is unlikely for at least two reasons. First of all, plastic accommodations due to the transformation strain will occur to a large extent in the softest phase, i.e. here in the austenite. This is the reason why its mean dislocation density increases drastically all along the transformation contrary to martensite. Secondly, higher degree of plastic interactions is expected after the percolation of the martensitic structure (about typically 20%-30% of transformation) [37,44]. Figure 3(b) shows on the contrary, a decrease in the rate of dislocation creation. As a consequence, we assume that the increase in the mean dislocation density in martensite is due the progressive nucleation of new laths containing more dislocations than the previous ones. Since the data are acquired all along the martensite phase transformation, it is possible to determine the dislocation density in these new laths, considering that the forming martensite lath is not affected by the earlier ones. It is also assumed that recovery process that could occur during martensite tempering is surely limited due to the applied cooling rate. However possible self-tempering (carbon segregation, carbide precipitation) cannot be ruled out even if no carbide can be observed and identified on the diffractograms.

In the following, we call the instantaneous dislocation density  $\rho^{\text{inst}}$  the dislocation density in the laths forming when the martensite fraction is F. At the beginning of the transformation, the instantaneous density is equal to the mean density of course. With what is said before, this

function progressively increases and contributes to increase the mean density of dislocations ( $\bar{\rho}$ ) in previously formed martensite F. By construction, it comes:

$$\bar{\rho} = 1/F \int_0^F \rho^{inst}(f) df \quad (2)$$

By deriving Equation (2) with respect to F, the instantaneous density of dislocations at F is given by:

$$d(F \bar{\rho}(F)) = \rho^{inst}(F) dF \quad (3)$$

Using a step by step integration, the instantaneous dislocation density for martensite is plotted in Figure 4.

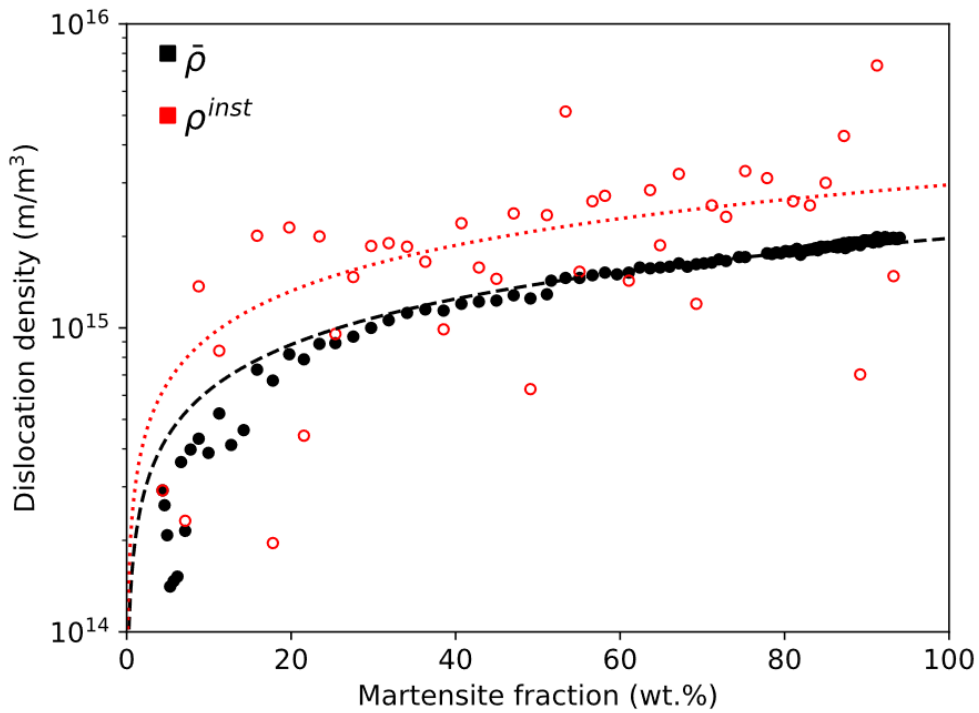


Figure 4: Mean dislocation density (filled circles) and instantaneous dislocation density calculated with ca. 2 wt.% steps (hollow circles) in martensite as a function of the martensite phase fraction during the quenching. The black discontinuous line corresponds to an empirical square-root law calibrated on the experimental results for a better readability of the results, while the red dotted continuous line corresponds to the analytical solution related to the empirical square-root law calibrated.

As the transformation moves forward, the new formed martensite laths contain a higher dislocation density than the earlier ones. This increase can be explained by the fact that the first martensite fraction is formed in a soft austenitic matrix. The following martensite laths would form in a harder matrix and with higher shearing modulus (temperature decrease) [12,27]. The inheritance of the austenite dislocation structure into martensite may also contribute to the total dislocation density in martensite. In fact, the final dislocation density in austenite at room temperature represents about 30% of the dislocation density expected in the very last formed laths of martensite.

#### Dislocations and strength of austenite

The dislocation density in the austenite before the martensitic transformation is of the order of  $10^{13} \text{ m/m}^3$  and increases with a rate higher than in the martensite during the transformation. For the austenite phase,  $\rho^{\text{inst}}$  is not presented as the increase in the mean dislocation density cannot reasonably be explained by a martensite transformation occurring solely in the dislocation poor austenitic grains. The increase results more probably from a progressive plasticization due to the accommodation of the transformation strains. However, it is likely that dislocations are not well and homogeneously distributed. This could explain in some extent the dispersions observed in the values at the beginning of the transformation.

The final dislocation density in austenite is  $1 \cdot 10^{15} \text{ m/m}^3$  at room temperature. This density is even higher than the ones found in the very first laths of martensite. Dislocations contribute to hardening, and this contribution  $\sigma_{\text{disl}}$ , can be calculated with the Taylor equation [45]:

$$\sigma_{\text{disl}} = \alpha C_T \mu b \rho^{-1/2} \quad (4)$$

where  $\alpha$  is a geometrical constant equal to 0.4,  $C_T$  the Taylor factor equal to 3,  $\mu$  is the shearing modulus (84 GPa),  $b$  and  $\rho$  are respectively the Burgers vectors ( $2.5 \cdot 10^{-10} \text{ m}$ ) of perfect dislocations in martensite and the mean dislocation density in austenite. The shear modulus was calculated at room temperature taking into account the steel composition [46].

The contribution to hardening of dislocations due to the martensitic transformation is thus equal to ca. 795 MPa in austenite. Retained austenite in martensite is thus far from being a soft phase, especially since the previous contribution does not account for solid solution hardening and size effect. In fact, retained austenite is often located as thin films in between martensite laths.

As a consequence, austenite cannot contribute to the plastic behavior of martensitic microstructures, at least not as much as supposed by certain models [47]. Retained austenite is in fact already intensively plasticized at room temperature due to the transformation strain and thus is also a hard phase of the microstructure.

#### Local and spatial yield strength distribution in martensite:

The instantaneous dislocation density shown in Figure 4 introduced a dislocation density distribution inside the martensite laths. The first formed at high temperatures (lower martensite fraction) show a lower dislocation density than those formed at lower temperature (higher martensite fraction). As a consequence, the contribution of dislocations to their respective hardening are surely different. Applying again the Taylor equation to the instantaneous density of dislocations instead of the average dislocation density permits to estimate the related distribution of strengths in the microstructure. The parameters used are  $\alpha=0.4$ ,  $C_T=3$ ,  $b=2.5 \cdot 10^{-10}\text{m}$ , and  $\mu$  the shearing modulus for a martensite with the initial steel composition (76 GPa). The method presented in the present work allows to estimate the dislocation hardening contribution to the yield strength in the forming martensite during the whole cooling, as shown in the Erreur : source de la référence non trouvée.

Erreur : source de la référence non trouvée(a) shows the dislocation contribution to the yield strength of the instantaneous dislocation density, for increasing  $F$  values. The Taylor equation was applied considering each instantaneous dislocation density while the newly formed phase fraction was summed to the total transformed martensite, allowing to show the increase of the dislocation strengthening with the martensite transformation. As expected, a similar trend with the instantaneous dislocation density in martensite phase is observed.

The dislocation contribution to the yield strength is two times higher in the last formed martensite lath than in the first one, respectively ca. 1250 and 500 MPa.

The density of probability of yielding at a given stress caused by the dislocations density distribution (called stress spectrum  $f(\sigma)$ ) was obtained by evaluating the dislocation hardening related to each newly formed martensite between the limits of 50 MPa bins from 0 to 4500 MPa. Once the bin in which the dislocation hardening belonged was identified (evaluated with the empirical root-law calculated instantaneous dislocation density, red dotted curve in Figure 4), the newly formed martensite fraction was summed to the fraction related to that interval.

By this method, at the end of the transformation, it was possible to obtain the total martensite fraction for each bin of 50 MPa. The following step was to normalize the integral of the fractions versus the local yield strength in order to obtain a distribution of probability which integral would be equal to 1 (the whole martensite transformed).

The mentioned density of probability has been plotted and presented Erreur : source de la référence non trouvée(b). The first spike in the obtained distribution is due to the fact that in the first calculated point the amount of fraction already transformed is significant.

The obtained distribution has been compared to the stress spectrum calculated by the Continuous Composite Approach (CCA) [2] to explain the behavior of the studied steels. The stress spectrum,  $f(\sigma)$ , in the CCA is obtained by reverse resolution of the following equation:

$$\Sigma = \int_{\sigma_{\min}}^{\sigma_L} f(\sigma) \sigma d\sigma + \sigma_L \int_{\sigma_L}^{+\infty} f(\sigma) d\sigma \quad (5)$$

where  $\Sigma$  is the macroscopic stress,  $\sigma_{\min}$  is the minimum value in the local yield stress spectrum,  $\sigma_L$  is the stress state of phases remaining elastic.

The CCA distribution presented in this work is obtained by the calculated tensile behavior of the studied alloy (0.215wt.% C) with [2]. In the CCA, all the contributions affect the distribution as solid solution strengthening due to carbon and substitutional alloying elements, friction of pure iron, internal stresses, dislocation densities. It explains the initial shift at higher strength of the distribution expected from the CCA compared to the distribution obtained by the dislocation density distribution alone. It also clearly appears that the ratio between the harder and the softer fraction formed (ca. 2.5 considering the dislocation distribution only) is lower than the actual ratio expected by the CCA model (ca. 6). The higher values of the density of probability of spectrum due to the dislocation hardening are due to that both curves are normalized and the lower ratio of this spectrum.

The lower ratio of the spectrum due to the dislocation density distribution means that the measured distributions of dislocations in martensite is not sufficient alone to explain the micromechanical behavior of the steel. Dislocation strengthening is not the sole contribution of the local yield of martensitic laths. As shown by Morsdorf et al. [9], the lath size effect must evidently be considered, but according to Badinier [10], the obtained spread of local yield is far from being sufficient to explain the stress spectrum. Different degrees of self-

tempering (carbide precipitation and carbon segregations) are also expected in martensite [48] but they cannot explain the behavior of martensite by themselves as shown by Hutchinson et al. [4].

Hutchinson et al. introduces calculated residual stress heterogeneities in the martensite (at the scale of the grains) resulting from the phase transformation during cooling to predict the tensile behavior of martensite microstructure [4]. The main assumption of the authors was to consider that the stress gradient contribution on the martensite FWHM is alone able to describe the martensite FWHM decrease during the tensile test as observed experimentally. However, it is well known that other contributions are present as tetragonality even for low carbon steels [49], crystallite size, dislocation density.

We consider that the distribution of flow stress (which could describe the stress-strain curve) in the martensite is originated by the microstructure principally (laths sizes, dislocations densities); internal stresses contribute to the phenomenon without being the only explanation as reported by Wang et al. [50]. Indeed, if the FWHMs are only due to the internal stresses and decrease with the further deformation (as reported by Hutchinson et al. [4]), the Bauschinger effect would decrease as well which is the opposite to the experimental observation [2,10,50].

Hence, it appears from this work that the local yield strength distribution in martensite is the result of a complex convolution of different mechanisms, having their own spatial distributions. However, it seems that the distribution of dislocation densities is one of the most important sources of spread (nearly one half of the distribution width), contrary to lath size distribution.

The functional form for the local yield stress spectrum in the CCA model (an Avrami type law [2]) can be selected differently based on the type of distribution found experimentally. However, for obtaining the real local yield stress spectrum not only the distribution of dislocation densities has to be considered, but also the other previously mentioned spatial distributions. The convolution of the mentioned distributions might produce a different type of functional form than the one that might be inferred only from the distribution of the dislocation densities. As consequence, the authors do not find convenient at the moment change the functional form, while the mentioned modification might be address subsequently while analyzing the other sources of distributions.

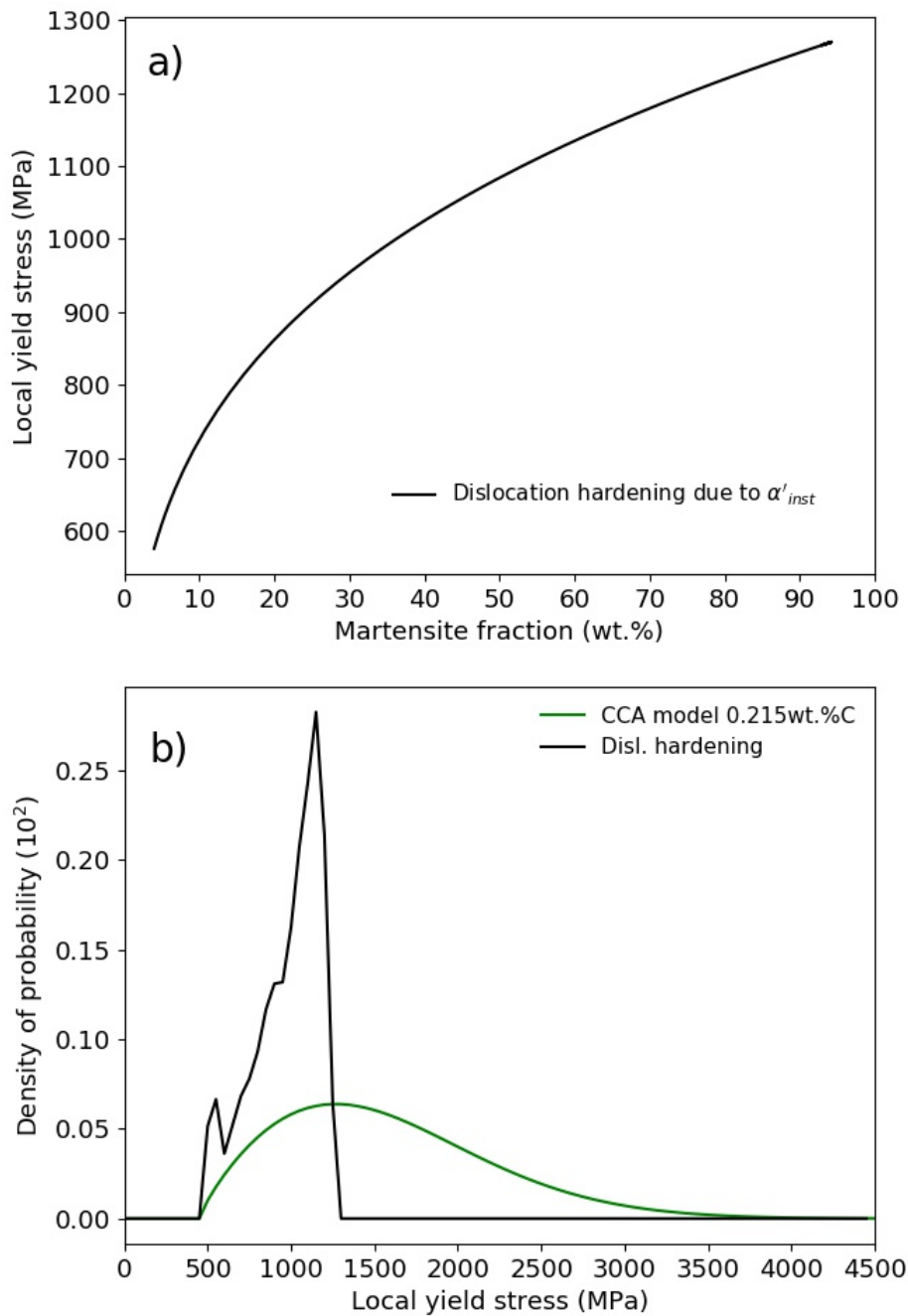


Figure 5: a) The dislocation contribution to the yield stress for each newly formed martensite fraction  
 b) The density probability to find a lath with a given local yield stress considering only the measured dislocation. These experimental values are compared to the expected stress distribution necessary to explain the mechanical behavior of the studied steel according to [2].

## **Conclusion**

The evolution of the dislocation densities in martensite and in austenite during the quench of a low-carbon (0.215wt.%C) steel has been investigated in situ by the mean of X-ray diffraction experiments on a synchrotron beamline. These measurements were conducted with the mWH methodology developed by Ungar et al. and a more conventional Rietveld refinement. The line configuration offers an excellent time resolution adapted to the kinetics of the studied steels.

The mean dislocations density in martensite was shown to increase progressively as the martensitic transformation proceeds confirming that dislocations are not homogeneously distributed between the laths, in agreement with recent post mortem observations. The resulting spatial distribution has been estimated introducing the concept of instantaneous dislocation density in martensite. The associated spread in the local yield strengths of laths has been compared to the one calculated on a micromechanical basis (CCA approach), i.e. based on an inverse analysis from the macroscopic mechanical behavior. It was shown that microstructural heterogeneities (dislocation densities, lath sizes, carbon segregations) as well as internal stresses resulting from the transformation deformation must be taken into account to explain the unique behavior of these steels [50]. The density of dislocations appears to be a major contribution explaining almost one half of the stress distribution.

The evolution of the dislocation density in austenite has also been analyzed in details and discussed at the light of the martensite transformation strains. Low carbon martensitic steels contain significant fraction of retained austenite but this latter phase cannot be considered as a soft phase as it contains almost the same density of dislocations as the martensite. The strength of retained austenite is necessarily higher than the softest martensite lath as it contains 10 times higher density of dislocations. Hence, retained austenite cannot be considered as the interphase medium permitting to explain the plastic deformation of martensitic microstructures (if excluding TRIP effect).

## **Acknowledgements**

This work was funded by the i-SITE Lorraine Université d'Excellence program (LUE) and supported by ArcelorMittal Maizières les Metz (Product Research Centre). The HEXRD experiments were conducted at DESY (PETRAIII-P07 beamline) in Hamburg under the I-20180973 EC grant. A special thanks is dedicated to the team of the P-07 line. The expertise

of N. Schell and A. Stark was much appreciated and widely contributed to the success of the study.

The Laboratory of Excellence on Design of Alloy Metals for low-mAss Structures (Labex DAMAS) from the Université de Lorraine (France) is also fully acknowledged for its support.

### **Conflicts of Interest**

The authors declare no conflict of interest. The funders had no role in the design of the study; in the collection, analyses, or interpretation of data; in the writing of the manuscript, or in the decision to publish the results.

### **Data availability**

The raw/processed data required to reproduce these findings cannot be shared at this time as the data also forms part of an ongoing study.

### **References**

- [1] N. Fonstein, *ADVANCED HIGH STRENGTH SHEET STEELS: physical metallurgy, design, processing, and properties.*, SPRINGER, 2016.
- [2] S. Allain, O. Bouaziz, M. Takahashi, Toward a New Interpretation of the Mechanical Behaviour of As-quenched Low Alloyed Martensitic Steels, *ISIJ Int.* 52 (2012) 717–722. <https://doi.org/10.2355/isijinternational.52.717>.
- [3] T. Ungár, S. Harjo, T. Kawasaki, Y. Tomota, G. Ribárik, Z. Shi, Composite Behavior of Lath Martensite Steels Induced by Plastic Strain, a New Paradigm for the Elastic-Plastic Response of Martensitic Steels, *Metall. Mater. Trans. A Phys. Metall. Mater. Sci.* 48 (2017) 159–167. <https://doi.org/10.1007/s11661-016-3845-4>.
- [4] B. Hutchinson, P. Bate, D. Lindell, A. Malik, M. Barnett, P. Lynch, Plastic yielding in lath martensites – An alternative viewpoint, *Acta Mater.* 152 (2018) 239–247. <https://doi.org/10.1016/j.actamat.2018.04.039>.
- [5] J. Li, T. Ohmura, K. Tsuzaki, Microstructure effect on nanohardness distribution for medium-carbon martensitic steel, *Sci. China, Ser. E Technol. Sci.* 49 (2006) 10–19. <https://doi.org/10.1007/s11431-004-5228-0>.
- [6] B.B. He, M.X. Huang, Revealing the Intrinsic Nanohardness of Lath Martensite in Low Carbon Steel, *Metall. Mater. Trans. A Phys. Metall. Mater. Sci.* 46 (2015) 688–694. <https://doi.org/10.1007/s11661-014-2681-7>.

- [7] B.B. He, K. Zhu, & M.X. Huang, On the nanoindentation behaviour of complex ferritic phases, *Philos. Mag. Lett.* (2014). <https://doi.org/10.1080/09500839.2014.921348>.
- [8] L. Morsdorf, O. Jeannin, D. Barbier, M. Mitsuhashi, D. Raabe, C.C. Tasan, Multiple mechanisms of lath martensite plasticity, *Acta Mater.* 121 (2016) 202–214. <https://doi.org/10.1016/j.actamat.2016.09.006>.
- [9] L. Morsdorf, C.C. Tasan, D. Ponge, D. Raabe, 3D structural and atomic-scale analysis of lath martensite: Effect of the transformation sequence, *Acta Mater.* 95 (2015) 366–377. <https://doi.org/10.1016/j.actamat.2015.05.023>.
- [10] G. Badinier, Effect of Carbon Segregation and Carbide Precipitation on the Mechanical Response of Martensite, University of British Columbia, 2013. <https://doi.org/10.14288/1.0073612>.
- [11] G. Badinier, C.W. Sinclair, X. Sauvage, X. Wang, V. Bylik, M. Gouné, F. Danoix, Microstructural heterogeneity and its relationship to the strength of martensite, *Mater. Sci. Eng. A.* 638 (2015) 329–339. <https://doi.org/10.1016/j.msea.2015.04.088>.
- [12] F. Christien, M.T.F. Telling, K.S. Knight, Neutron diffraction in situ monitoring of the dislocation density during martensitic transformation in a stainless steel, *Scr. Mater.* 68 (2013) 506–509. <https://doi.org/10.1016/j.scriptamat.2012.11.031>.
- [13] G. Ashiotis, A. Deschildre, Z. Nawaz, J.P. Wright, D. Karkoulis, F.E. Picca, J. Kieffer, The fast azimuthal integration Python library: PyFAI, *J. Appl. Crystallogr.* 48 (2015) 510–519. <https://doi.org/10.1107/S1600576715004306>.
- [14] S. Allain, S. Aoued, A. Quintin-Poulon, M. Gouné, F. Danoix, J.-C. Hell, M. Bouzat, M. Soler, G. Geandier, In Situ Investigation of the Iron Carbide Precipitation Process in a Fe-C-Mn-Si Q&P Steel, *Materials (Basel)*. 11 (2018) 1087. <https://doi.org/10.3390/ma11071087>.
- [15] G.K. Williamson, W.H. Hall, X-ray line broadening from filed aluminium and wolfram, *Acta Metall.* 1 (1953) 22–31. [https://doi.org/10.1016/0001-6160\(53\)90006-6](https://doi.org/10.1016/0001-6160(53)90006-6).
- [16] N. Sallel, X. Boulnat, A. Borbély, J.L. Béchade, D. Fabrègue, M. Perez, Y. De Carlan, L. Hennet, C. Mocuta, D. Thiaudière, Y. Bréchet, In situ characterization of microstructural instabilities: Recovery, recrystallization and abnormal growth in nanoreinforced steel powder, *Acta Mater.* 87 (2015) 377–389. <https://doi.org/10.1016/j.actamat.2014.11.051>.
- [17] P.S.-Iuc.M. on Crystallography, undefined 1993, *The Rietveld Method*, edited by RA Young, (n.d.).

- [18] T. Ungár, A. Borbély, The effect of dislocation contrast on x-ray line broadening: A new approach to line profile analysis, *Appl. Phys. Lett.* 69 (1996) 3173–3175. <https://doi.org/10.1063/1.117951>.
- [19] N. Sallel, X. Boulmat, A. Borbély, J.L. Béchade, D. Fabrègue, M. Perez, Y. De Carlan, L. Hennet, C. Mocuta, D. Thiaudière, Y. Bréchet, In situ characterization of microstructural instabilities: Recovery, recrystallization and abnormal growth in nanoreinforced steel powder, *Acta Mater.* 87 (2015) 377–389. <https://doi.org/10.1016/j.actamat.2014.11.051>.
- [20] T. Ungár, I. Dragomir, Á. Révész, A. Borbély, The contrast factors of dislocations in cubic crystals: the dislocation model of strain anisotropy in practice, *J. Appl. Crystallogr.* 32 (1999) 992–1002. <https://doi.org/10.1107/s0021889899009334>.
- [21] T. Ungár, G. Tichy, The Effect of Dislocation Contrast on X-Ray Line Profiles in Untextured Polycrystals, *Phys. Status Solidi.* 171 (1999) 425–434. [https://doi.org/10.1002/\(SICI\)1521-396X\(199902\)171:2<425::AID-PSSA425>3.0.CO;2-W](https://doi.org/10.1002/(SICI)1521-396X(199902)171:2<425::AID-PSSA425>3.0.CO;2-W).
- [22] S. Takaki, T. Masumura, T. Tsuchiyama, Proposal of simplified modified Williamson-Hall equation, *ISIJ Int.* 58 (2018) 2354–2356. <https://doi.org/10.2355/isijinternational.ISIJINT-2018-517>.
- [23] Z.M. Shi, W. Gong, Y. Tomota, S. Harjo, J. Li, B. Chi, J. Pu, Study of tempering behavior of lath martensite using in situ neutron diffraction, *Mater. Charact.* 107 (2015) 29–32. <https://doi.org/10.1016/j.matchar.2015.06.040>.
- [24] A. Borbély, J. Dragomir-Cernatescu, G. Ribárik, T. Ungár, Computer program ANIZC for the calculation of diffraction contrast factors of dislocations in elastically anisotropic cubic, hexagonal and trigonal crystals, *J. Appl. Crystallogr.* 36 (2003) 160–162. <https://doi.org/10.1107/S0021889802021581>.
- [25] J. Leese, A.E. Lord, Elastic stiffness coefficients of single-crystal iron from room temperature to 500°C, *J. Appl. Phys.* 39 (1968) 3986–3988. <https://doi.org/10.1063/1.1656884>.
- [26] D.J. Dever, Temperature dependence of the elastic constants in  $\alpha$ -iron single crystals: Relationship to spin order and diffusion anomalies, *J. Appl. Phys.* 43 (1972) 3293–3301. <https://doi.org/10.1063/1.1661710>.
- [27] D.G. Isaak, K. Masuda, Elastic and viscoelastic properties of  $\alpha$  iron at high temperatures, *J. Geophys. Res.* 100 (1995). <https://doi.org/10.1029/95jb01235>.

- [28] Y. Zhao, L. Le Joncour, A. Baczmański, E. Gadalińska, S. Wroński, B. Panicaud, M. François, C. Braham, T. Buslaps, Stress distribution correlated with damage in duplex stainless steel studied by synchrotron diffraction during plastic necking, *Mater. Des.* 113 (2016) 157–168. <https://doi.org/10.1016/j.matdes.2016.10.014i>.
- [29] H.S. Yang, H.K.D.H. Bhadeshia, Uncertainties in dilatometric determination of martensite start temperature, *Mater. Sci. Technol.* 23 (2007) 556–560. <https://doi.org/10.1179/174328407X176857>.
- [30] S.M.C. van Bohemen, J. Sietsma, The kinetics of bainite and martensite formation in steels during cooling, *Mater. Sci. Eng. A.* 527 (2010) 6672–6676. <https://doi.org/10.1016/j.msea.2010.06.091>.
- [31] S.M.C. van Bohemen, L. Morsdorf, Predicting the Ms temperature of steels with a thermodynamic based model including the effect of the prior austenite grain size, *Acta Mater.* 125 (2017) 401–415. <https://doi.org/10.1016/j.actamat.2016.12.029>.
- [32] S.M.C. van Bohemen, Bainite and martensite start temperature calculated with exponential carbon dependence, *Mater. Sci. Technol.* 28 (2012) 487–495. <https://doi.org/10.1179/1743284711Y.0000000097>.
- [33] H.K.D.H. Bhadeshia, Thermodynamic extrapolation and martensite-start temperature of substitutionally alloyed steels, *Met. Sci.* 15 (1981) 178–180. <https://doi.org/10.1179/030634581790426697>.
- [34] Y. Wang, Y. Tomota, T. Ohmura, S. Morooka, W. Gong, S. Harjo, Real time observation of martensite transformation for a 0.4C low alloyed steel by neutron diffraction, *Acta Mater.* 184 (2020) 30–40. <https://doi.org/10.1016/j.actamat.2019.11.051>.
- [35] A.A.P. K. SIPOS, L. REMY, A. Q.P. Analysis, Influence of Austenite Predeformation on Mechanical Properties and Strain-Induced Martensitic Transformations of a High Manganese Steel, *Metall. Trans. A.* 7 (1976).
- [36] N. Nakada, Y. Ishibashi, T. Tsuchiyama, S. Takaki, Self-stabilization of untransformed austenite by hydrostatic pressure via martensitic transformation, *Acta Mater.* 110 (2016) 95–102. <https://doi.org/10.1016/j.actamat.2016.03.048>.
- [37] S.Y.P. Allain, S. Gaudez, G. Geandier, J.C. Hell, M. Gouné, F. Danoix, M. Soler, S. Aoued, A. Poulon-Quintin, Internal stresses and carbon enrichment in austenite of Quenching and Partitioning steels from high energy X-ray diffraction experiments, *Mater. Sci. Eng. A.* 710 (2018) 245–250. <https://doi.org/10.1016/j.msea.2017.10.105>.

- [38] M. Dehmas, F. Bruneseaux, G. Geandier, E. Gautier, B. Appolaire, S. Denis, B. Denand, A. Settefrati, A. Mauro, M. Peel, G. Gonzales Aviles, T. Buslaps, Apport de la diffraction synchrotron à l'étude de la transformation martensitique dans les aciers, *Matériaux Tech.* 97 (2009) 61–69. <https://doi.org/10.1051/mattech/2010012>.
- [39] F. Archie, M.Z. Mughal, M. Sebastiani, E. Bemporad, S. Zaefferer, Anisotropic distribution of the micro residual stresses in lath martensite revealed by FIB ring-core milling technique, *Acta Mater.* 150 (2018) 327–338. <https://doi.org/10.1016/j.actamat.2018.03.030>.
- [40] D. Fukui, N. Nakada, S. Onaka, Internal residual stress originated from Bain strain and its effect on hardness in Fe–Ni martensite, *Acta Mater.* 196 (2020) 660–668. <https://doi.org/10.1016/j.actamat.2020.07.013>.
- [41] S. Morito, J. Nishikawa, T. Maki, Dislocation Density within Lath Martensite in Fe–C and Fe–Ni Alloys, *ISIJ Int.* 43 (2003) 1475–1477. <https://doi.org/10.2355/isijinternational.43.1475>.
- [42] G. Krauss, Martensite in steel: strength and structure, *Mater. Sci. Eng. A.* 273–275 (1999) 40–57. [https://doi.org/10.1016/S0921-5093\(99\)00288-9](https://doi.org/10.1016/S0921-5093(99)00288-9).
- [43] D.C. Saha, E. Biro, A.P. Gerlich, Y. Zhou, Effects of tempering mode on the structural changes of martensite, *Mater. Sci. Eng. A.* 673 (2016) 467–475. <https://doi.org/10.1016/j.msea.2016.07.092>.
- [44] S. Nambu, N. Shibuta, M. Ojima, J. Inoue, T. Koseki, H.K.D.H. Bhadeshia, In situ observations and crystallographic analysis of martensitic transformation in steel, *Acta Mater.* 61 (2013) 4831–4839. <https://doi.org/10.1016/j.actamat.2013.04.065>.
- [45] G.I. Taylor, Plastic Strain in Metals, *J. Inst. Met.* 62 (1938) 307–.
- [46] G. Ghosh, G.B. Olson, The isotropic shear modulus of multicomponent Fe-base solid solutions, *Acta Mater.* 50 (2002) 2655–2675. [https://doi.org/10.1016/S1359-6454\(02\)00096-4](https://doi.org/10.1016/S1359-6454(02)00096-4).
- [47] F. Maresca, V.G. Kouznetsova, M.G.D. Geers, Deformation behaviour of lath martensite in multi-phase steels, *Scr. Mater.* 110 (2016) 74–77. <https://doi.org/10.1016/j.scriptamat.2015.08.004>.
- [48] B. Hutchinson, J. Hagström, O. Karlsson, D. Lindell, M. Tornberg, F. Lindberg, M. Thuvander, Microstructures and hardness of as-quenched martensites (0.1–0.5%C), *Acta Mater.* 59 (2011) 5845–5858. <https://doi.org/10.1016/j.actamat.2011.05.061>.
- [49] N. Maruyama, S. Tabata, H. Kawata, Excess Solute Carbon and Tetragonality in As-

Quenched Fe-1Mn-C (C:0.07 to 0.8 Mass Pct) Martensite, *Metall. Mater. Trans. A Phys. Metall. Mater. Sci.* 51 (2020) 1085–1097. <https://doi.org/10.1007/s11661-019-05617-y>.

- [50] L.Y. Wang, Y.X. Wu, W.W. Sun, Y. Bréchet, L. Brassart, A. Arlazarov, C.R. Hutchinson, Strain hardening behaviour of as-quenched and tempered martensite, *Acta Mater.* (2020). <https://doi.org/10.1016/j.actamat.2020.08.067>.

### **Supplementary data**

Three experiments were conducted to assess the reproducibility. All the experiments were investigated as describe in the present paper. The FWHM evolutions and mean dislocation density are shown for both martensite and austenite phases during the cooling treatment. In addition the mean dislocation and instantaneous dislocation densities were also show. As one experiment were detailed in the paper, here only the two other experiments results are displayed.

### Experience 1

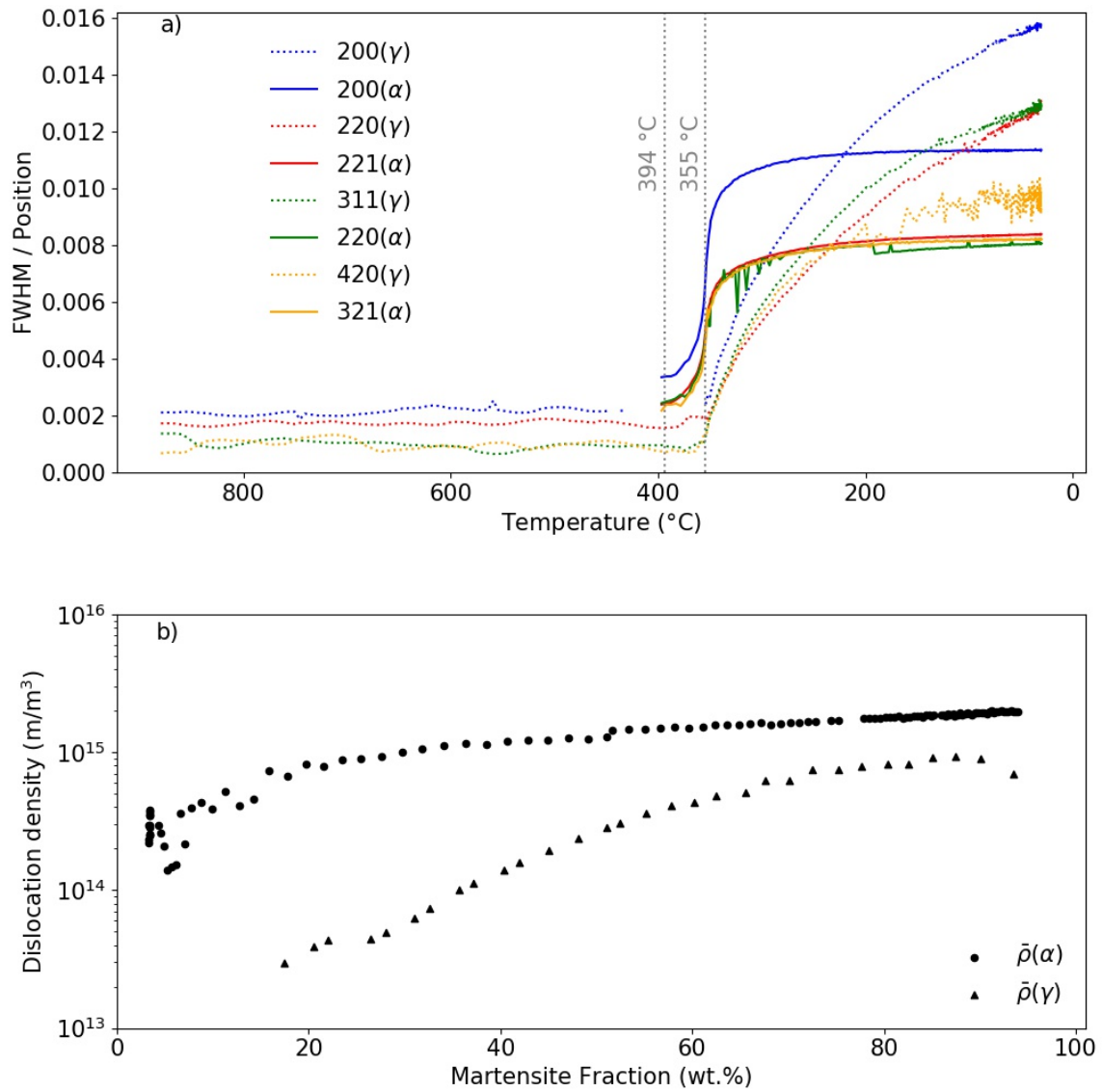


Figure 6: a) FWHMs of austenite (dotted lines) and martensite (continuous lines) diffraction peaks as function of the temperature during the whole studied cooling sequence (after austenitization down to room temperature) and b) deduced mean dislocation densities in both martensite (circle) and austenite (triangles) as a function of the transformed martensite phase fraction.

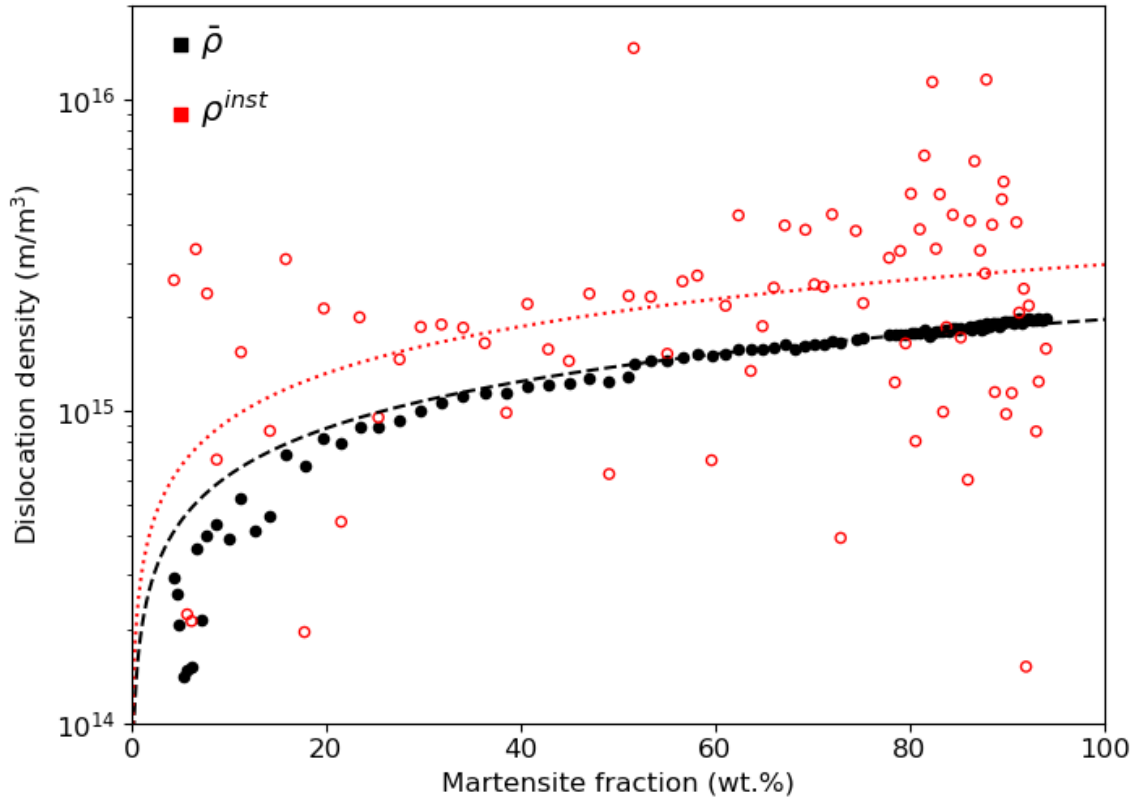


Figure 7: Mean dislocation density (filled circles) and instantaneous dislocation density (hollow circles) in martensite as a function of the martensite phase fraction during the quenching. The black discontinuous line corresponds to an empirical square-root law calibrated on the experimental results for a better readability of the results, while the red dotted continuous line corresponds to the analytical solution related to the empirical square-root law calibrated.

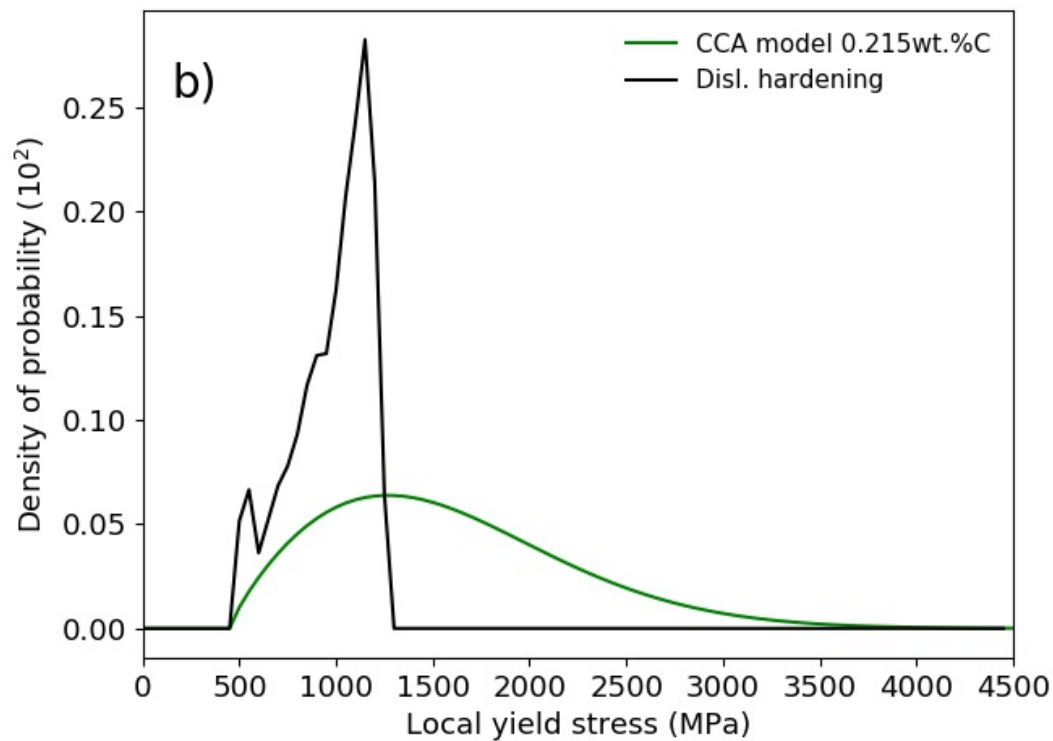
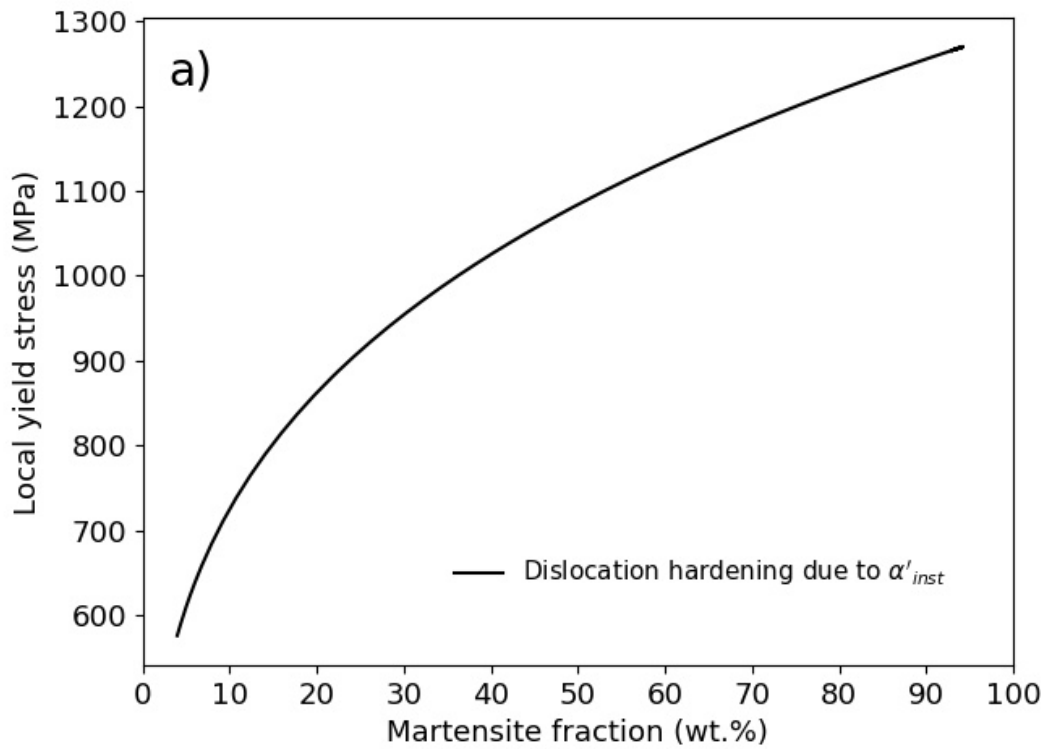


Figure 8: a) The dislocation contribution to the yield stress for each newly formed martensite fraction  
 b) The density probability to find a lath with a given local yield stress considering only the measured dislocation. These experimental values are compared to the expected stress distribution necessary to explain the mechanical behavior of the studied steel according to [2].

## Experience 2

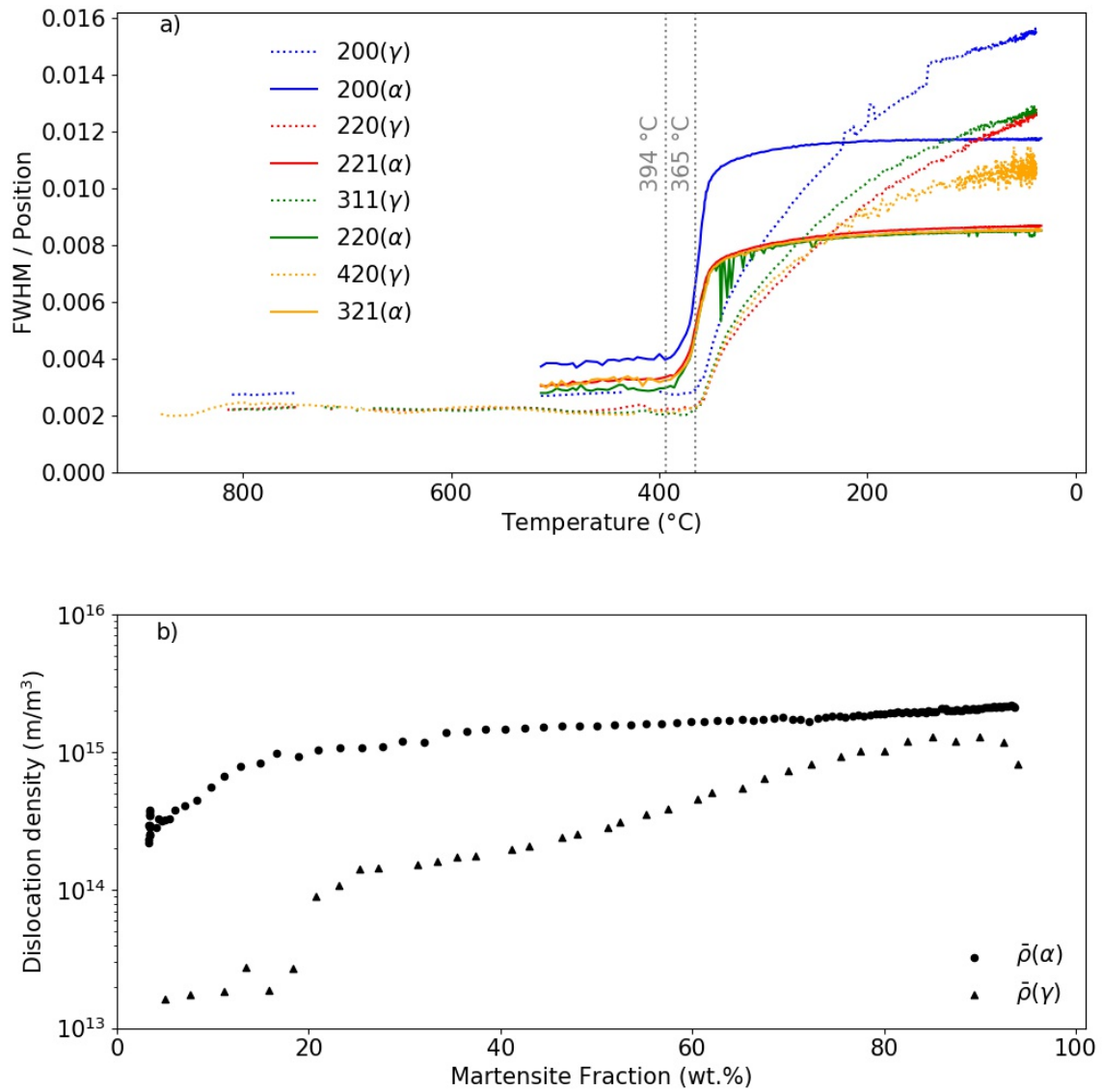


Figure 9: a) FWHMs of austenite (dotted lines) and martensite (continuous lines) diffraction peaks as function of the temperature during the whole studied cooling sequence (after austenitization down to room temperature) and b) deduced mean dislocation densities in both martensite (circle) and austenite (triangles) as a function of the transformed martensite phase fraction.

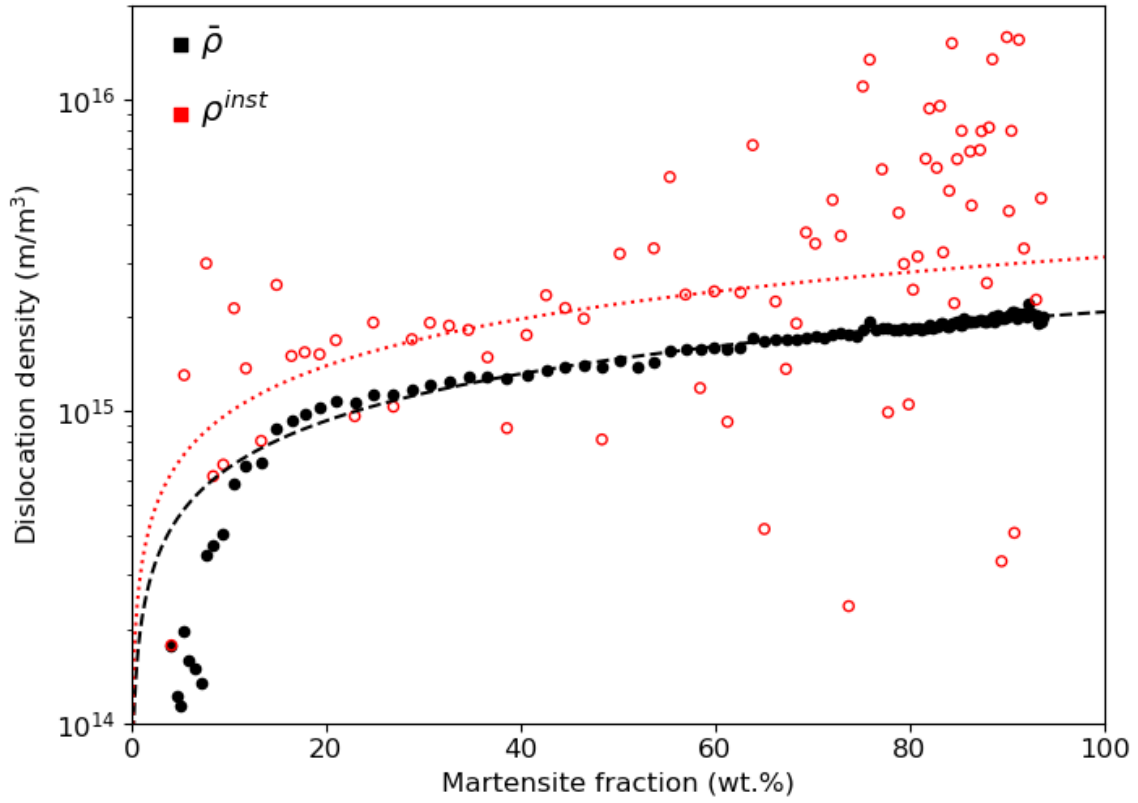


Figure 10: Mean dislocation density (filled circles) and instantaneous dislocation density (hollow circles) in martensite as a function of the martensite phase fraction during the quenching. The black discontinuous line corresponds to an empirical square-root law calibrated on the experimental results for a better readability of the results, while the red dotted continuous line corresponds to the analytical solution related to the empirical square-root law calibrated.

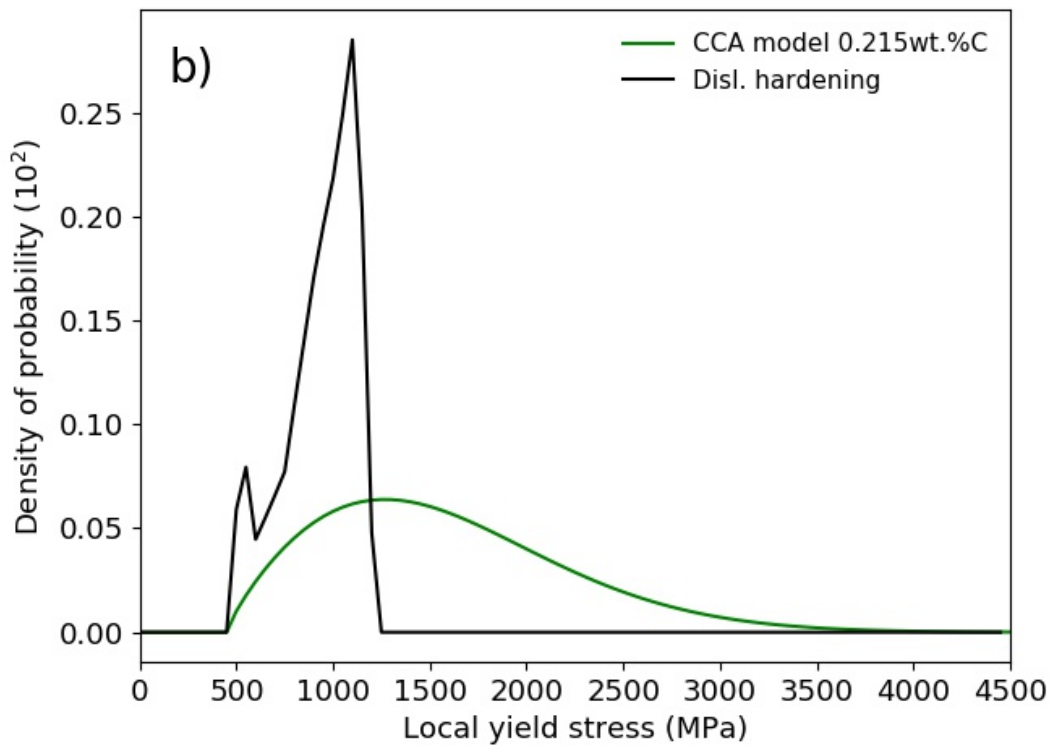
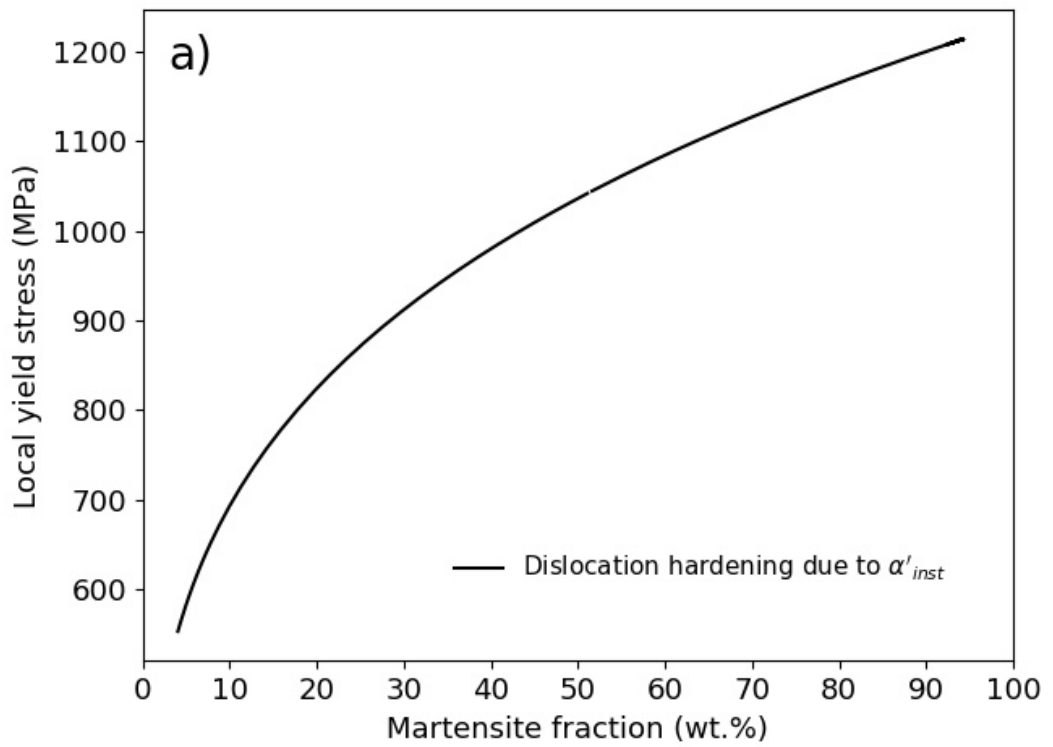


Figure 11: a) The dislocation contribution to the yield stress for each newly formed martensite fraction  
 b) The density probability to find a lath with a given local yield stress considering only the measured dislocation. These experimental values are compared to the expected stress distribution necessary to explain the mechanical behavior of the studied steel according to [2].